

Chiral magnetic structure of spin-ladder multiferroic BaFe₂Se₃W. G. Zheng,¹ V. Balédent,¹ E. Ressouche,² V. Petricek,³ D. Bounoua,⁴ P. Bourges,⁴ Y. Sidis,⁴ A. Forget,⁵ D. Colson,⁵ and P. Foury-Leylekian^{1,*}¹Université Paris-Saclay, CNRS, Laboratoire de Physique des Solides, 91405 Orsay, France²Université Grenoble Alpes, CEA, IRIG, MEM, MDN, 38000 Grenoble, France³Department of Structure Analysis, Institute of Physics, Praha, Czech Republic⁴Université Paris-Saclay, CNRS-CEA, Laboratoire Léon Brillouin, 91191 Gif sur Yvette, France⁵Université Paris-Saclay, CEA, CNRS, SPEC, 91191 Gif-sur-Yvette, France

(Received 6 July 2022; accepted 26 September 2022; published 24 October 2022)

The determination of accurate magnetic structure of magnetoelectric materials is a mandatory key step to understand their properties. In order to couple to the lattice and induce an electric polarization, this structure is unfortunately complex in most cases, and results from magnetic frustration, either geometrical or exchange in nature. The compound BaFe₂Se₃ is one of the rare quasi-one-dimensional compounds that exhibits such magnetoelectric properties. In this paper, thanks to a single crystal neutron diffraction study and symmetry analysis, an umbrellalike magnetic structure has been revealed, with tilted moments in the (*a*, *c*) and (*b*, *c*) planes, confirmed by polarized neutron diffraction. It corresponds to a magnetic order with antiferromagnetic blocks and a propagation vector $k = (\frac{1}{2}, \frac{1}{2}, \frac{1}{2})$, belonging to the *C₄m* magnetic space group. This work should allow further theoretical studies of the coupling of this magnetic order with the lattice and the ferroelectric order. It also provides key information on the magnetism, of which fluctuations may be at the origin of the pressure-induced superconductivity in this family.

DOI: [10.1103/PhysRevB.106.134429](https://doi.org/10.1103/PhysRevB.106.134429)**I. INTRODUCTION**

Mn-based compounds have long been the main source of magnetoelectric systems with improper ferroelectricity. Indeed, their multiple stable valences, as well as their high magnetic moment for 3*d* ions allow one to produce type-II multiferroicity, where ferroelectricity is induced by the establishment of a magnetic order. The families *RMnO₃* and *RMn₂O₅* (*R* being a rare earth) are the archetypes of these materials, presenting a large magnetoelectric coupling. However, these properties are limited to low temperature, generally below 50 K [1]. The research of such properties has thus turned to iron-based compounds. This interest is motivated by the fact that iron presents the same advantages as Mn (large magnetic moment and multiple valences), with generally higher magnetic order temperatures due to stronger magnetic exchange interactions, above 100 K [2]. In this context we studied the quasi-one-dimensional (quasi-1D) Fe spin ladder BaFe₂Se₃ and evidenced a polar structure at room temperature [3] as well as a magnetoelectric coupling at the Néel temperature (200 K). This compound derives from the famous iron-based superconductors, and can be seen as stripes of two-dimensional FeSe [4], forming ladders. Interestingly, a superconducting state appears in BaFe₂Se₃ above a pressure of 10 GPa which is proposed to be driven by the magnetic fluctuations [5]. The determination of the exact magnetic structure in this compound is of utmost importance, to understand both the microscopic processes at the origin of the multiferroicity

and the superconductivity mechanism expected to be related to magnetic fluctuations of the neighboring ordered phase.

The crystal structure of BaFe₂Se₃ is shown in Fig. 1(a). It crystallizes in the average *Pnma* space group [unit cell parameters for this orthorhombic O1 phase : $a_{O1} = 11.878(3)$ Å, $b_{O1} = 5.447(2)$ Å, $c_{O1} = 9.160(2)$ Å] [6]. In each unit cell, there are two Fe ladders (ladder A and ladder B) which are built of edge-sharing FeSe₄ tetrahedra propagating along the *b* axis.

Below $T_N = 225 \pm 25$ K, BaFe₂Se₃ undergoes a magnetic transition which has been investigated by a variety of powder neutron diffraction (PND) experiments as well as simulations [7–11]. The ordered moments reach $2.8\mu_B$ by Fe [8] at low temperature, which is smaller than the value of $4\mu_B$ expected for Fe²⁺ moments. In the magnetic phase, we have shown recently by x-ray diffraction that the space group of the nuclear phase is *Pm* (unit cell parameters: $a_{M1} = 9.1496$ Å, $b_{M1} = 5.4489$ Å, $c_{M1} = 11.8673$ Å, $\beta_{M1} = 90.031^\circ$) [3]. The symmetry breaking from *Pnma* was also observed by transmission electron microscopy [12] and lattice dynamic study [13]. However, it is important to note that it is very weak. Thus the average structure has been used in first intention to determine the magnetic space group in order not to miss possible quasiasymmetries.

As for the magnetic order, it is a blocklike antiferromagnetic (AFM) state with moments along the *a* axis and a propagation vector $(\frac{1}{2}, \frac{1}{2}, \frac{1}{2})$. Along the ladders, the up-up-down-down spin pattern of the blocklike AFM structure is the fingerprint of a magnetic frustration issued from competing exchange interactions present in the system [14]. However, the accurate magnetic structure is still not solved due to the limi-

*Corresponding author: pascale.foury@u-psud.fr

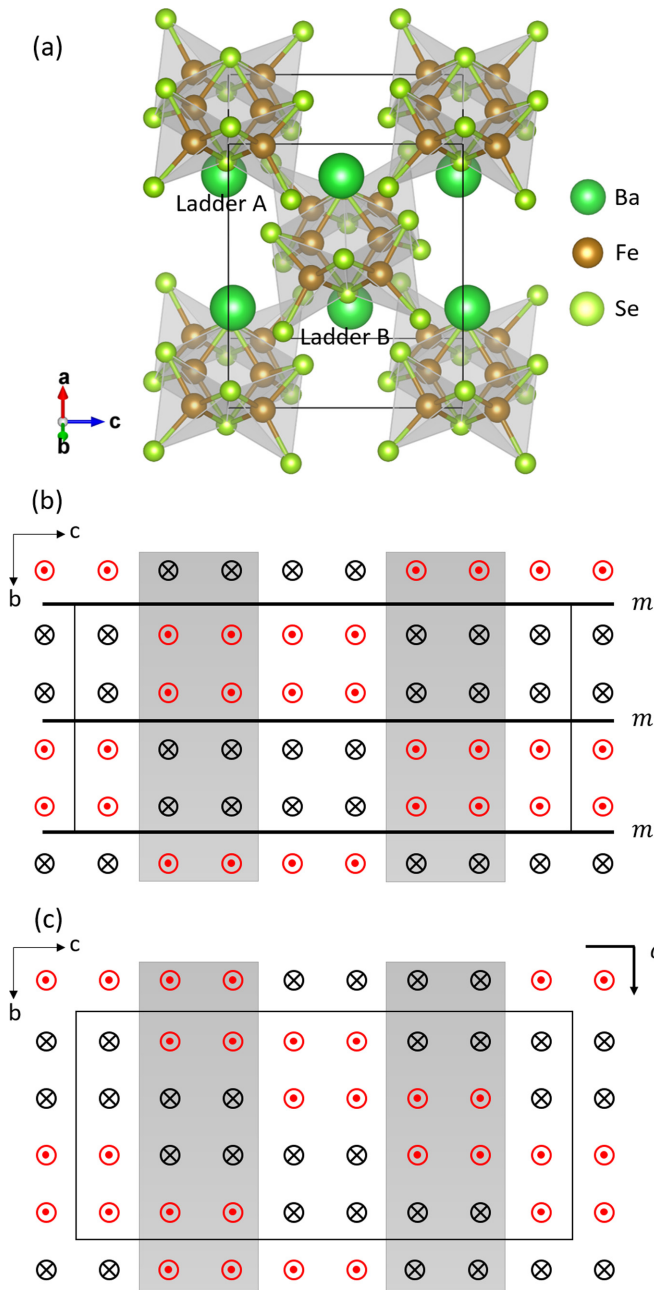


FIG. 1. (a) Crystallographic structure of BaFe₂Se₃ in the *Pnma* space group. (b) and (c) Projections of the Fe atoms on the *bc* plane of block-A (b) and block-B (c) magnetic orders. The *m* mirror of *C₂am* (block A) and *c* glide plane of *C₂ac* (block B) are shown. The spins are perpendicular to the *bc* plane. The black rectangles indicate the magnetic unit cell. The Fe ladders A (B) are represented by white (gray) strips.

tation of diffraction on powder. Indeed, PND experiments are not accurate enough to give information on an eventual canting of the spins, as proposed by certain authors. The authors of Ref. [7] propose a block-A magnetic order [Fig. 1(b)] while those of Refs. [8,9] propose a block-B structure [Fig. 1(c)]. The difference relies on the fact that the ferromagnetic 2×2 superblocks between ladder A and ladder B are antiferromagnetically ordered in the block-A model while there is a phase

shift of only one Fe-Fe distance between them in the block-B model. A first-principles study found that the energy per Fe for the block-B structure is the lowest among the various magnetic models tested [11]. However, the difference between block A and block B is only 7.9 meV/Fe, which is close to the error bars of density functional theory (DFT) calculations. The lack of reliable magnetic structure avoids further progress in the understanding of the remarkable physical properties of BaFe₂Se₃ [9,15]. In this work, we aim at studying its accurate magnetic order by single-crystal neutron diffraction and polarized neutron scattering. Our accurate determination of the magnetic structure would pave the way for further investigations of the mechanism of stabilization of the multiferroic character as well as on the competition between magnetism and superconductivity.

II. EXPERIMENTAL DETAILS

BaFe₂Se₃ crystals were grown from the melt using the self-flux method [16]. The crystal was grown starting from a stoichiometric mixture of Ba (99.9%) pieces, powder of Fe (99.9%), and Se (99.999%) with Ba : Fe : Se = 1 : 2 : 3. Two grams of reagents were pelletized, placed in a carbon crucible, and then sealed in an evacuated quartz tube with partial pressure of 300 mbar of Ar gas. The quartz tube was placed in a vertical tubular furnace, annealed to 1150 °C, first cooled down to 750 °C at 6°/h and finally down to room temperature.

The starting mixture for crystal growth was prepared using small pieces of Ba (99.9%), powder of Fe (99.9%), and Se (99.999%). Two grams of reagents were weighed, mixed with the composition 1 : 2 : 3. The resulting pellets were placed in a carbon crucible and then sealed in an evacuated quartz tube with partial pressure of 300 mbar of Ar gas. Single-crystal neutron diffraction experiments were carried out on the thermal CEA-CRG D23 single-crystal diffractometer at the Institut Laue Langevin (Grenoble, France) with an incident wavelength $\lambda = 2.36$ Å selected by a focusing PG 002 monochromator. The crystal was mounted in a closed-cycle refrigerator in four-circle geometry, and data collection was performed at 10 K. A standard aluminum holder was used to mount the sample and to cool it down. Refinement of both the nuclear and magnetic structures was performed by the JANA2006 program [17]. In addition, single-crystal polarized neutron diffraction was performed on the 4F1 triple axis spectrometer at Orphée reactor (Saclay, France). The incident wavelength was set to $\lambda = 2.57$ Å and the spin polarization of the incident beam was realized by a bender with a transmission $T = 0.5$ at this wavelength. The crystal was cooled down to 5 K using a closed-cycle helium cryostat.

III. SYMMETRY ANALYSIS

The determination of the correct magnetic space group is an essential starting point to study the magnetic structure. We used the *k*-SUBGROUPSMAG program of the Bilbao Crystallographic Server [18]. From the room temperature space group *Pnma* and considering the magnetic propagation vector $k = (\frac{1}{2}, \frac{1}{2}, \frac{1}{2})$ measured below T_N , three magnetic subgroups are possible : *C₂ac*, *C₂am*, and *P₂1*. Since the last space group is

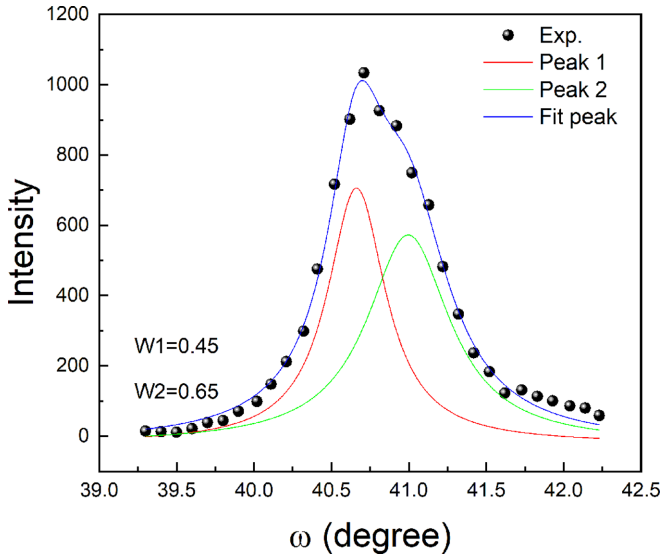


FIG. 2. Rocking (ω) scan of the (4 0 4) nuclear reflection at 10 K. The black circles are experimental data, and the colorful lines are the fitting results with a Lorentzian distribution.

of low symmetry, we first focused on the two others and would come back to it as a last resort. As shown in Fig. 1, block-A and block-B magnetic orders satisfy C_{4m} or C_{4c} symmetries, respectively. Therefore, the determination of the magnetic space group automatically fix the nature of the block-type order. As the magnetic group should necessarily be a subgroup of Pm , a simple symmetry analysis directly excludes the magnetic space group C_{4c} and thus the block-B magnetic order. Note that this is a different conclusion from other analyses based on the average space group $Pnma$ [19].

IV. SINGLE CRYSTAL X-RAY DIFFRACTION EXPERIMENT

To further progress in the accurate determination of the magnetic structure, we performed a single-crystal neutron diffraction measurement down to 10 K. The sample used was a $5 \times 2 \times 1$ mm³ specimen carefully characterized as described in Ref. [3] and with $T_N = 210$ K \pm 10 K, compatible with previous papers [8,9,16,20]. The quality of the sample was checked with a rocking (ω) scan of selected nuclear reflections. The scan of the (4 0 4) reflection at 10 K is shown in Fig. 2. Two peaks with a FWHM of 0.45° and 0.65°, respectively, indicate the presence of at least two crystallites. This is intrinsic to the morphology of the crystals related to the quasi-1D character of the system. The single crystals are indeed constituted of multiple needles roughly aligned along the b axis. Although the specimen is not a perfect single crystal, it is enough to determine the magnetic structure by neutron diffraction measurement. A data collection of 376 reflections, including 128 nuclear and 248 magnetic reflections, was recorded at 10 K. A space group test was performed for nuclear reflections. The internal R factor for the $P1m1$ space group is 7%, which is the best possible considering the experimental data. With the initial atomic positions from Ref. [3], we obtained at 10 K the structure shown in the Table I

TABLE I. Positions of the Fe ions and their moments in BaFe₂Se₃ at 10 K in the double- $Pnma$ setting ($R_{obs} = 9.16\%$). (For more details see the Supplemental Material.)

Atom	x	y	z	M_x	M_y	M_z
Fe1_1_1	-0.3714	0.1321	-0.1763	2.13	0.68	1.26
Fe1_1_2	0.3716	0.3651	0.0737	2.13	-0.68	-1.26
Fe1_2_1	0.1214	0.1281	0.1763	2.13	0.68	-1.26
Fe1_2_2	-0.1216	0.3701	0.4263	2.13	-0.68	1.26

of the Supplemental Material [21] with a reliability factor $R(obs) = 2.08\%$.

As mentioned above, the Cam magnetic space group and block-A magnetic order is the only one compatible with the nuclear Pm group and the observed propagation wave vector $(\frac{1}{2}, \frac{1}{2}, \frac{1}{2})$. We refined the magnetic structure and to facilitate the comparison with the average $Pnma$ setting, we used a double- $Pnma$ setting (the orthorhombic doubled unit cell is labeled O2, $a_{O2} = 23.7346$ Å, $b_{O2} = 10.8978$ Å, and $c_{O2} = 18.2992$ Å). The transformation matrices are presented in the Supplemental Material (Fig. 1) as well as the details of the refinements. We first refined the magnetic structure with all Fe³⁺ magnetic moments identical in magnitude and along a . This is not required by the symmetry constraints of Cam but corresponds to the magnetic orders proposed in previous works [7,8]. We obtained a magnetic R factor of $R(obs) = 16.83\%$ and $M_x = 2.33\mu_B$ per Fe with the twin fraction $t_{wvol2} = 0.5001$ (see Supplemental Material for details). The amplitude of the moments is slightly smaller than the value previously published [8].

We then authorized the rotation of the moments around the a axis. The best magnetic R factor we got was $R(obs) = 9.16\%$ (Table I). The comparison between the structure factors observed and calculated with this model is shown in Fig. 3. The results of the refinement are listed in Table II. One can see that the moments are tilted from the a axis by 18° in the ab plane and by 30° in the ac plane. Figure 4(a) shows the projections of the Fe atoms and their spins on the bc plane. As one can see, the spins of each block form an umbrella-type structure. The net moment of each block is only along the a axis and antiferromagnetically arranged along the b axis. It is important to notice that the spins are nearly along the apical direction of the tetrahedra (the maximum deviation of the moments from the Fe-Se bonds is 20°) [Fig. 4(b)]. This could be the indication of an easy axis of the Fe spins in its local tetrahedral environment as observed in certain systems [22].

V. POLARIZED NEUTRON SCATTERING

We decided to employ polarized neutron diffraction to address the question of the canting of the moments in order to validate our model. The single-crystal polarized neutron experiment has been performed on the triple-axis instrument 4F1 installed at the LLB-Orphée reactor (the polarized neutron setup on 4F1 could be found in Ref. [23]). In addition, we used at the sample position the μ -PAD device available on 4F1 to access the full polarization matrix. The scattering plane was (1,1,0) and (0,0,1) defining the basis x', y', z' with

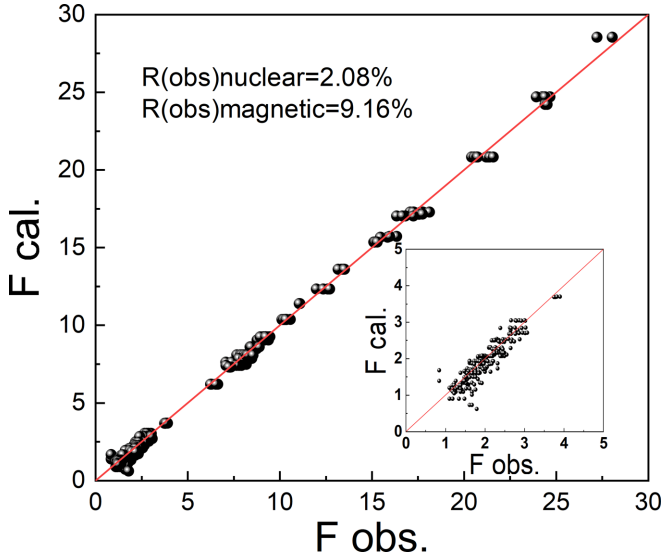


FIG. 3. Result of the refinement for the C_m magnetic structure. Structure factors of nuclear and magnetic Bragg reflections collected at 10 K are plotted against the calculated values. The inset shows the range of low F value which mainly represents the magnetic reflections.

x' along \vec{Q} , y' perpendicular to \vec{Q} in the scattering plane, and z' the direction perpendicular to the scattering plane. We performed a full neutron polarization analysis on the (1,1,1) Bragg reflection at 150 K and the $(\frac{1}{2}, \frac{1}{2}, \frac{1}{2})$ at both 60 and 5 K. Following a procedure to analyze the neutron polarization described in [24], we extracted six relevant terms: the nuclear term (N), the moment along y' and z' ($M_{y'}$ and $M_{z'}$), the chiral term (M_{ch}), and the nuclear-magnetic interference terms ($R_{y'}$ and $R_{z'}$) using the following equations:

$$\begin{aligned}
 N &= \sigma_{x',x'}^{++} = \sigma_{x',x'}^{--}, \\
 M_{y'} &= \frac{\sigma_{y',y'}^{++} + \sigma_{y',y'}^{--}}{2} - \frac{\sigma_{x',x'}^{++} + \sigma_{x',x'}^{--}}{2}, \\
 &= \frac{\sigma_{x',x'}^{+-} + \sigma_{x',x'}^{-+}}{2} - \frac{\sigma_{y',y'}^{+-} + \sigma_{y',y'}^{-+}}{2}, \\
 M_{z'} &= \frac{\sigma_{z',z'}^{++} + \sigma_{z',z'}^{--}}{2} - \frac{\sigma_{x',x'}^{++} + \sigma_{x',x'}^{--}}{2}, \\
 &= \frac{\sigma_{x',x'}^{+-} + \sigma_{x',x'}^{-+}}{2} - \frac{\sigma_{z',z'}^{+-} + \sigma_{z',z'}^{-+}}{2}, \\
 M_{ch} &= \frac{\sigma_{x',x'}^{+-} - \sigma_{x',x'}^{-+}}{2P_0}, \\
 R_y &= \frac{\sigma_{y',y'}^{++} - \sigma_{y',y'}^{--}}{2P_0}, \\
 R_z &= \frac{\sigma_{z',z'}^{++} - \sigma_{z',z'}^{--}}{2P_0}
 \end{aligned} \tag{1}$$

with $\sigma_{s_i, s_f}^{\text{sign}_i, \text{sign}_f}$ the intensity of the incident and final spin along the direction s_i and s_f , respectively, sign_i and sign_f the sign + or - of the incident and final spin projection along this axis, and P_0 the polarization of the beam (+1 or -1). These

TABLE II. Relative intensity of the terms extracted from the full polarization analysis on the (1,1,1) nuclear Bragg at 150 K, the (0.5,0.5,0.5) Bragg at 60 and 5 K, and calculation of these terms from refined magnetic structure at 10 K.

(h, k, l)	(1,1,1)	$(\frac{1}{2}, \frac{1}{2}, \frac{1}{2})$	$(\frac{1}{2}, \frac{1}{2}, \frac{1}{2})$	$(\frac{1}{2}, \frac{1}{2}, \frac{1}{2})$
Temperature	150 K	60 K	5 K	10 K (calc.)
N	0.26(1)	0.012(1)	0.020(4)	0
$M_{y'}$	0.001(1)	0.085(3)	0.109(4)	0.07
$M_{z'}$	-0.004(3)	0.363(2)	0.42(3)	0.54
M_{ch}	0.002(1)	0.008(2)	-0.049(3)	0.32
$R_{y'}$	0.005(2)	0.002(1)	-0.011(1)	0
$R_{z'}$	0.001(1)	0.010(1)	-0.044(2)	0

six terms for the $(\frac{1}{2}, \frac{1}{2}, \frac{1}{2})$ reflection are calculated with the magnetic model of BaFe_2Se_3 issued from our refinement. The results are presented in Table II. As can be seen, only the nuclear term is nonzero on the (1,1,1) nuclear Bragg peak at 150 K as expected for a purely nuclear reflection. At low temperature, the ratio between the $M_{z'}$ and $M_{y'}$ amplitudes of the magnetic reflection $(\frac{1}{2}, \frac{1}{2}, \frac{1}{2})$ is around 4 confirming that the moments are tilted away from the a axis as a moment purely along a would give a ratio above 20 according to simulations. In addition, this ratio decreases between 60 and 5 K, showing that the tilt is more pronounced at lower temperature. This ratio enables one to discriminate between several magnetic structures giving a satisfying R factor. The structure proposed in Fig. 4 gives $M_{z'}$ and $M_{y'}$ terms which are the closest to the experimental ones from polarized neutron diffraction with a

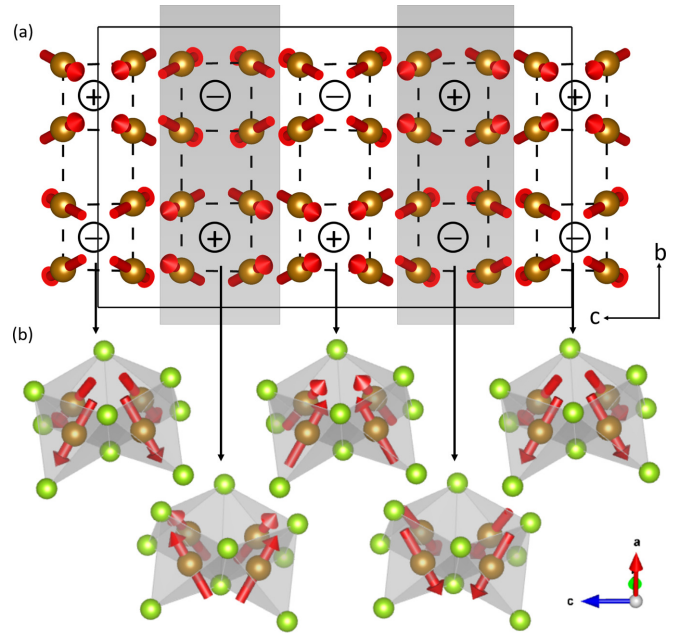


FIG. 4. (a) Projections of the Fe atoms on the bc plane with the tilting spins in block-A magnetic order. The yellow balls indicate the Fe atoms and the red arrows are the spins of Fe. The + and - indicate the net moments of the blocks. The Fe ladder A (B) is represented by a white (gray) background. (b) The FeSe_4 tetrahedra of the blocks in (a) (indicated by the black arrows).

ratio M_z/M_y calculated around 7 ± 1 and measured around 4 ± 1 (see Table I).

As for the chiral term M_{ch} which is nonzero at 5 K, it can be explained by the chirality of the proposed structure, Fig. 4. Two enantiomorphs are related by inversion symmetry. In the case of a single chiral domain, we calculate that M_{ch} would have nearly half the value of M_z for the $(\frac{1}{2}, \frac{1}{2}, \frac{1}{2})$ Bragg reflection. The much smaller value measured for M_{ch} in the experiment (see Table II) is likely due to the presence of chiral domains. By comparison of the calculation with the experiment of Table II, we estimate the chiral twin factor to 0.57. Interestingly, we can see that the chiral term loses 85% of its 5 K value at 60 K. This effect cannot be ascribed to the decrease of the ordered moment since the M_z and M_y amplitudes only drop by nearly 20% in the same range of temperature, but rather to a spin reorganization. Interestingly, the vanishing of M_{ch} is accompanied by the decreasing of the ratio between M_z and M_y (4.3 for 60 K and 3.8 for 5 K). Indeed, chirality would be absent for a collinear structure with moments purely along a . As the moments are further tilted at low temperature, the chirality increases, as observed experimentally. It appears that the nuclear-magnetic terms and the chiral term are linked, suggesting that the tilted spins and chirality play a central role in the multiferroic properties of this material. Indeed the presence of such chirality and noncollinearity may have a strong implication on the magnetoelectric coupling, bringing into play the Dzyaloshinskii-Moriya interaction, for example.

Concerning the experimental values of N , R_y , and R_z measured for the $(\frac{1}{2}, \frac{1}{2}, \frac{1}{2})$ reflection, they are found to be very small but sizable at 5 K. These nuclear-magnetic interference terms could not be calculated with our model since only the magnetic structure was considered. After warming up to 60 K, these terms strongly decrease but remain finite. Such terms are usually very difficult to measure and rarely observed experimentally due to the existence of domains which are canceling these nuclear-magnetic terms. The fact that these terms are observable is remarkable and may provide a possible proof of a strong coupling between the lattice and the magnetism in this multiferroic compound that goes beyond the scope of this paper.

VI. DISCUSSION

We determined here the accurate magnetic order of the challenging spin-ladder compound, BaFe_2Se_3 , by a combi-

nation of single-crystal neutron diffraction combined with spherical polarization analysis. We show that the exact structure is the AFM block-A type. This result confirms the blocklike magnetic order previously determined from powder neutron diffraction. This order strongly differs from the structure of the parent system BaFe_2S_3 . The unusual character of the block arrangement has been recently explained by the ladder distortion evidenced in [3]. This distortion is characterized by a tetramerization of the Fe ladder which creates an alternation of larger and smaller squarelike Fe plaquettes [13] and thus a block character. The block-A magnetic order evidenced by our work is of great interest regarding the multiferroic properties. Indeed, according to [25], the block-A (labeled block-MF by Dong *et al.*) should lead to a strong electric polarization by an exchange-striction mechanism involving the Fe and Se atoms. Due to the particular magnetic phase shift between ladders, the electric moments created by the two ladders of the unit cell are cooperative and produce a strong net electric polarization along a . We also evidenced a canting of the spins with respect to the a axis of about 30° and 18° in the ac and ab planes, respectively. This canting does not produce any ferromagnetic component along b or c and the net moment is only aligned along a . Interestingly, the spin orientation is roughly along one apical direction which could be the easy axis of the Fe spin in its tetrahedral environment. This interpretation, if validated by DFT calculations, could indicate that the anisotropy factor may over to exchange couplings involved in this system. This canting induces a spin chirality, and is accompanied with an increase of the spin-lattice coupling as observed in the off-diagonal term of the polarization matrix. This work thus provides key information to elucidate the microscopic mechanism responsible for the magnetoelectric coupling in relationship with the chirality and its link to the spin-lattice coupling. It also gives hints on the underlying magnetic interactions, of which fluctuations and dynamics are likely to be responsible for the pressure-induced superconductivity.

ACKNOWLEDGMENTS

Experiments at ILL were sponsored by the French Neutron Federation (2FDN), with data references from Proposal. This work was financially supported by the ANR COCOM 20-CE30-0029. This work was also supported by a CSC scholarship (No. 201806830111).

-
- [1] S. Chattopadhyay, V. Balédent, F. Damay, A. Gukasov, E. Moshopoulou, P. Auban-Senzier, C. Pasquier, G. André, F. Porcher, E. Elkaim *et al.*, *Phys. Rev. B* **93**, 104406 (2016).
- [2] S. M. Disseler, J. A. Borchers, C. M. Brooks, J. A. Mundy, J. A. Moyer, D. A. Hillsberry, E. L. Thies, D. A. Tenne, J. Heron, M. E. Holtz *et al.*, *Phys. Rev. Lett.* **114**, 217602 (2015).
- [3] W. Zheng, V. Balédent, M. B. Lepetit, P. Retailleau, E. V. Elslande, C. R. Pasquier, P. Auban-Senzier, A. Forget, D. Colson, and P. Foury-Leylekian, *Phys. Rev. B* **101**, 020101(R) (2020).
- [4] F.-C. Hsu, J.-Y. Luo, K.-W. Yeh, T.-K. Chen, T.-W. Huang, P. M. Wu, Y.-C. Lee, Y.-L. Huang, Y.-Y. Chu, D.-C. Yan, and M.-K. Wu, *Proc. Natl. Acad. Sci. USA* **105**, 14262 (2008).
- [5] W.-G. Zheng, V. Baledent, C. V. Colin, F. Damay, J.-P. Rueff, A. Forget, D. Colson, and P. Foury-Leylekian, *Commun. Phys.* **5**, 183 (2022).
- [6] H. Hong and H. Steinfink, *J. Solid State Chem.* **5**, 93 (1972).
- [7] A. Krzton-Maziopa, E. Pomjakushina, V. Pomjakushin, D. Sheptyakov, D. Chernyshov, V. Svitlyk, and K. Conder, *J. Phys.: Condens. Matter* **23**, 402201 (2011).

- [8] J. M. Caron, J. R. Neilson, D. C. Miller, A. Llobet, and T. M. McQueen, *Phys. Rev. B* **84**, 180409(R) (2011).
- [9] Y. Nambu, K. Ohgushi, S. Suzuki, F. Du, M. Avdeev, Y. Uwatoko, K. Munakata, H. Fukazawa, S. Chi, Y. Ueda, and T. J. Sato, *Phys. Rev. B* **85**, 064413 (2012).
- [10] Q. Luo, A. Nicholson, J. Rincón, S. Liang, J. Riera, G. Alvarez, L. Wang, W. Ku, G. D. Samolyuk, A. Moreo, and E. Dagotto, *Phys. Rev. B* **87**, 024404 (2013).
- [11] Y. Zhang, L.-F. Lin, J.-J. Zhang, E. Dagotto, and S. Dong, *Phys. Rev. B* **97**, 045119 (2018).
- [12] K. Du, L. Guo, J. Peng, X. Chen, Z.-N. Zhou, Y. Zhang, T. Zheng, Y.-P. Liang, J.-P. Lu, Z.-H. Ni *et al.*, *npj Quantum Mater.* **5**, 49 (2020).
- [13] M. J. Weseloh, V. Balédent, W. Zheng, M. Verseils, P. Roy, J. B. Brubach, D. Colson, A. Forget, P. Foury-Leylekian, and M. B. Lepetit, *J. Phys.: Condens. Matter* **34**, 255402 (2022).
- [14] M. Mourigal, S. Wu, M. B. Stone, J. R. Neilson, J. M. Caron, T. M. McQueen, and C. L. Broholm, *Phys. Rev. Lett.* **115**, 047401 (2015).
- [15] J. Ying, H. Lei, C. Petrovic, Y. Xiao, and V. V. Struzhkin, *Phys. Rev. B* **95**, 241109(R) (2017).
- [16] H. Lei, H. Ryu, A. I. Frenkel, and C. Petrovic, *Phys. Rev. B* **84**, 214511 (2011).
- [17] V. Petříček, M. Dušek, and L. Palatinus, *Z. Kristall.-Cryst. Mater.* **229**, 345 (2014).
- [18] J. Perez-Mato, S. Gallego, E. Tasci, L. Elcoro, G. de la Flor, and M. Aroyo, *Annu. Rev. Mater. Res.* **45**, 217 (2015).
- [19] S. W. Lovesey, D. D. Khalyavin, and G. van der Laan, *Phys. Scr.* **91**, 015803 (2016).
- [20] J. Gao, Y. Teng, W. Liu, S. Chen, W. Tong, M. Li, X. Zhao, and X. Liu, *RSC Advances* **7**, 30433 (2017).
- [21] See Supplemental Material at <http://link.aps.org/supplemental/10.1103/PhysRevB.106.134429> for details of the nuclear and magnetic structure at low temperature, as well as the transformation matrix between the nuclear unit cell and the magnetic one.
- [22] J. Nehr Korn, I. A. Valuev, M. A. Kiskin, A. S. Bogomyakov, E. A. Suturina, A. M. Sheveleva, V. I. Ovcharenko, K. Holldack, C. Herrmann, M. V. Fedin *et al.*, *J. Mater. Chem. C* **9**, 9446 (2021).
- [23] V. Balédent, D. Haug, Y. Sidis, V. Hinkov, C. T. Lin, and P. Bourges, *Phys. Rev. B* **83**, 104504 (2011).
- [24] L. P. Regnault, H. M. Rønnow, C. Boullier, J. E. Lorenzo, and C. Marin, *Phys. B: Condens. Matter* **345**, 111 (2004).
- [25] S. Dong, J.-M. Liu, and E. Dagotto, *Phys. Rev. Lett.* **113**, 187204 (2014).